# Application of resonators and a side branch duct with an expansion chamber for broad band noise control

Haluk Erol[a] and Cem Meriç[b]

(Received: 5 January 2009; Revised: 27 April 2009; Accepted: 28 April 2009)

**One way of attenuating broad band noise that propagates through ducts or pipe systems is to use one or more reactive-type acoustic components, each of which is specifically designed for optimal performance at a particular frequency range. This paper uses the transfer matrix method for predicting the transmission loss (TL) of a system with resonators connected to the main duct and a side branch duct modified with a zero-mean-flow expansion chamber. The method is applied to different configurations, and the numerical predictions are compared with the results obtained using finite element methods. Our results indicate that broadband resonators and a side branch duct with an expansion chamber, fitted as a countermeasure for broadband noise, can offer significant benefits.**


Primary subject classification: 37.6; Secondary subject classification: 34

## 1 INTRODUCTION

In intake systems of internal combustion engines, side branch-type mufflers are often used, for example, for turbocharger noise control. Two types of noise generally occur in turbochargers—blowing or whooshing noise, and pulsation noise at frequencies of about 1000–3000 Hz. The resulting noise can be very audible both inside and outside the vehicle.

Recent advances in modeling and accurate performance prediction have led to the development of simulation methods for practical muffler components in commercial design. Muffler designers need simple, fast and accurate modeling tools, especially in the preliminary design evaluation stages. Finite element and boundary element methods are often used to provide valid results over a wide range of frequencies. However, these methods are time-consuming, they require highly trained personnel, and the commercial software is usually expensive. Therefore, plane wave-based models, such as the transfer matrix method, can quickly offer initial prototype solutions for muffler designers. However, we note that the transfer matrix method has a limited frequency range.

A resonator can be an effective acoustic attenuation device at low frequencies. Recently, Selamet and co-workers employed several approaches to examine Helmholtz resonator applications[1–4]. The Helmholtz resonator is considered one of the most efficient tuning methods and is widely used in vehicle exhaust and intake systems. Modifications have been made to improve the acoustic attenuation of the Helmholtz resonator. Birdsong and Radcliff proposed a smart Helmholtz resonator for use in the vehicle intake system[5]. In addition to a Helmholtz resonator, the Herschel-Quincke (HQ) tube is a simple implementation of the interference principle in an acoustic attenuation device. Considering the application of HQ tubes to systems such as compressors and the intake and exhaust systems of internal combustion engines, the effect of a mean flow is not negligible. Selamet et al. modeled the HQ tube, removed many of the geometric restrictions associated with previous work and examined innovative new approaches[6]. Using a three-dimensional model that took into account the curvature of the HQ tube, they determined that, with just a plane wave, the one-dimensional model (which approximates the tube as being straight) is sufficient. Selamet and Radavich then examined a side branch expansion chamber in the context of an HQ tube[7]. They investigated how geometrical variation of the side branch and HQ tube influenced the resonant frequencies of the system. Another innovative use of the HQ tube by Selamet and Easwaran was to extend the previous analysis of the two-duct HQ tube without flow[8]. They found closed form solutions for the TL and resonance locations for the n-duct configurations. They also found that the additional branches increased the frequency band and the amount of noise attenuation. The effects of flow on the attenuation characteristics of different

[a] Mechanical Engineering, Istanbul Technical University, Gümüşsuyu, 34439, Istanbul TURKEY; email: erolha@itu.edu.tr.
[b] Mechanical Engineering, Istanbul Technical University, Gümüşsuyu, 34439, Istanbul TURKEY.

HQ tube configurations have been investigated by Fuller and Beis[9], Torregrosa et al.[10] and Zhichi et al.[11]. Peaks of high attenuation were seemingly reduced and shifted in the presence of flow. However, such publications only examined the effects of plane waves on the HQ tubes. In more complex systems the effects of higher order modes on the HQ tube system become very important. Brady et al. were the first to study the potential of HQ tubes for attenuating higher order modes in two-dimensional ducts[12]. Hallez et al. extended the two-dimensional analysis of higher order modes to three dimensions, i.e., hard-walled circular ducts[13]. Designs based on HQ tubes have been awarded many patents for reducing the exhaust noise of internal combustion engines and have been used in various practical problems. Strunk investigated a variation of the HQ tube for hydraulic systems used in off-road earth-moving vehicle fluid power systems[14]. Chen and Hastings used a variation of the HQ tube to examine its ability to reduce fluid-borne noise in power steering hydraulic transmission lines[15]. Gerges et al. used the transfer matrix method to predict the TL of a muffler system[16]. The first suggestion for the combined use of HQ tubes and quarter-wave resonators appeared in work by Trochon[17]. Another interesting implementation of the HQ concept is described by Graefenstein and Wenzel[18]. The basic theory of the HQ tube and recent contributions to the understanding of the acoustical behavior of HQ ducts is available elsewhere[19–21]. One of the most popular references on the acoustics of ducts and mufflers is the work of Munjal[22].

This paper uses the transfer matrix method to predict, with no mean flow, the TL of a system with two resonators connected to the main duct and a side branch duct modified with an expansion chamber. Resonators, in our analytical model, are connected to the main duct; however, by setting the diameter and length of the neck, the analytical model can be converted for direct connection scenarios. The transfer matrix method is applied to different configurations, and the numerical predictions are compared with results from finite element methods. We discuss the limitations of the plane wave approach. Furthermore, in this study, for optimal acoustic attenuation performance in the 1000–3000 Hz frequency range, we demonstrate a muffler tuned for the intake system of an internal combustion engine that features a turbocharger.

## 2 THEORY

Figure 1 shows a system diagram. All calculations assume that a 1D model is valid. This requires that the maximum duct diameters are sufficiently small for the investigated frequency range. If the duct diameter is less than half the wavelength, the waves in the duct can

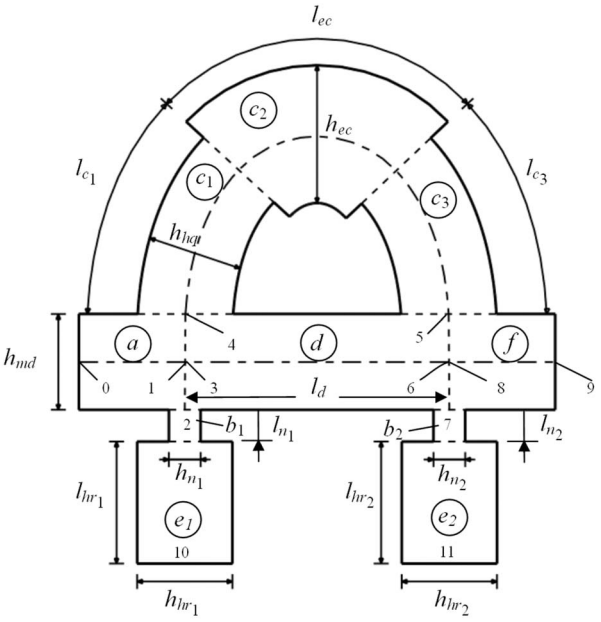


*Fig. 1—System with two resonators connected to the main duct and a side branch duct modified with an expansion chamber.*

be considered plane waves; this means that the 1D model for wave propagation is valid.

The rigid straight main duct has a constant cross section, and its diameter is $h_{md}$. The length of the main duct is $l_{md}$. The modified side branch duct connected to the main duct is also divided into 3 elements of lengths $l_{c_1}$, $l_{c_2}$ and $l_{c_3}$. The diameter of each element is $h_{hq}$, $h_{ec}$ and $h_{hq}$, as shown in Fig. 1. There are two resonators connected to the main duct. The neck diameters and lengths are $h_{n_1}$, $h_{n_2}$, $l_{n_1}$ and $l_{n_2}$. The resonator cavity lengths and diameters are $l_{hr_1}$, $l_{hr_2}$, $h_{hr_1}$ and $h_{hr_2}$. This study deals with the transfer matrix method for predicting, with zero mean flow, the TL of the system. Thus, the system shown in Fig. 1 is divided into 10 elements: a, $b_1$, $b_2$, $c_1$, $c_2$, $c_3$, d, $e_1$, $e_2$ and f.

Plane wave propagation in a rigid straight pipe with length $L$ can be described by its transmission (or four-pole) matrix, as follows:

$$\begin{bmatrix} p(0,t) \\ v(0,t) \end{bmatrix} = \begin{bmatrix} A & B \\ C & D \end{bmatrix} \begin{bmatrix} p(L,t) \\ v(L,t) \end{bmatrix}, \tag{1}$$

where $p(0,t)$, $p(L,t)$, $v(0,t)$ and $v(L,t)$ are the sound pressures and volume velocities at the input and the output; and $A$, $B$, $C$ and $D$ are four-pole parameters.

The sound pressure field inside the tube is

$$p(x,t) = p^{+} e^{\mathrm{i}(\omega t - kx)} + p^{-} e^{\mathrm{i}(\omega t + kx)}, \tag{2}$$

where $\mathrm{i} = \sqrt{-1}$, $\omega$ is the angular frequency in radians per second, $t$ is the time, $k$ is the wave number or propagation

constant, and $x$ is the plane wave propagation axis. Then the inlet pressure and volume velocity are

$$p(0,t) = (p^+ + p^-)e^{i\omega t}, \tag{3}$$

$$v(0,t) = \frac{(p^+ - p^-)e^{i\omega t}}{\rho c}, \tag{4}$$

and the output pressure and volume velocity are

$$p(L,t) = (p^+ e^{-ikL} + p^- e^{ikL})e^{i\omega t}, \tag{5}$$

$$v(L,t) = \frac{(p^+ e^{-ikL} - p^- e^{ikL})e^{i\omega t}}{\rho c}, \tag{6}$$

where $\rho$ is the density, and c is the speed of sound.

Thus, from Eqns. (3)–(6)

$$\begin{bmatrix} p(L) \\ v(L) \end{bmatrix} = \begin{bmatrix} \cos(kL) & -i\dfrac{\rho c}{S}\sin(kL) \\ -i\dfrac{S}{\rho c}\sin(kL) & -\cos(kL) \end{bmatrix} \begin{bmatrix} p(0) \\ v(0) \end{bmatrix}. \tag{7}$$

Equation (7) can be rearranged as

$$\begin{bmatrix} p(0) \\ v(0) \end{bmatrix} = \begin{bmatrix} \cos(kL) & i\dfrac{\rho c}{S}\sin(kL) \\ i\dfrac{S}{\rho c}\sin(kL) & \cos(kL) \end{bmatrix} \begin{bmatrix} p(L) \\ v(L) \end{bmatrix}, \tag{8}$$

and then

$$\mathbf{T} = \begin{bmatrix} A & B \\ C & D \end{bmatrix} = \begin{bmatrix} \cos(kL) & i\dfrac{\rho c}{S}\sin(kL) \\ i\dfrac{S}{\rho c}\sin(kL) & \cos(kL) \end{bmatrix} \tag{9}$$

is the transfer matrix of the rigid straight pipe. Here, S is the cross sectional area of the acoustic domains.

The description of the subsystems in terms of their four-pole parameters is very convenient, because the output of one system is the input of the next, from which it follows that the transmission matrix of a system that features multiple cascaded subsystems can be formulated in matrix form as

$$\begin{bmatrix} p_0 \\ v_0 \end{bmatrix} = \mathbf{T}_a \mathbf{T}_{18} \mathbf{T}_f \begin{bmatrix} p_9 \\ v_9 \end{bmatrix}$$

or

$$\begin{bmatrix} p_0 \\ v_0 \end{bmatrix} = \begin{bmatrix} A_a & B_a \\ C_a & D_a \end{bmatrix} \begin{bmatrix} A_{18} & B_{18} \\ C_{18} & D_{18} \end{bmatrix} \begin{bmatrix} A_f & B_f \\ C_f & D_f \end{bmatrix} \begin{bmatrix} p_9 \\ v_9 \end{bmatrix}, \tag{10}$$

where $\mathbf{T}_{18}$ is the transfer matrix of the system between the inlet "element a" and the outlet "element f."

For "element a," the relations between the sound pressures and the volume velocities are represented by four-pole parameters as

$$\begin{bmatrix} p_0 \\ v_0 \end{bmatrix} = \mathbf{T}_a \begin{bmatrix} p_1 \\ v_1 \end{bmatrix}, \tag{11}$$

where junction points 0 and 1 are the input and the output of "element a," respectively.

For "element c," the relations between the sound pressures and the volume velocities are represented by four-pole parameters as $A_c$, $B_c$, $C_c$ and $D_c$

$$\begin{bmatrix} p_4 \\ v_4 \end{bmatrix} = \mathbf{T}_c \begin{bmatrix} p_5 \\ v_5 \end{bmatrix}, \tag{12}$$

where $\mathbf{T}_c$ is the transfer matrix of the side branch duct modified with an expansion chamber, which can be expressed as the multiplication of the transfer matrices of each of the elements $c_1$, $c_2$, and $c_3$, as

$$\mathbf{T}_c = \mathbf{T}_{c_1} \mathbf{T}_{c_2} \mathbf{T}_{c_3} = \begin{bmatrix} A_c & B_c \\ C_c & D_c \end{bmatrix}. \tag{13}$$

Then, for "element f," the relations between the sound pressures and the volume velocities are represented by four-pole parameters as

$$\begin{bmatrix} p_8 \\ v_8 \end{bmatrix} = \mathbf{T}_f \begin{bmatrix} p_9 \\ v_9 \end{bmatrix}, \tag{14}$$

where junction points 8 and 9 are the input and the output of "element f," respectively.

Similarly, for "element d," the relations between the sound pressures and the volume velocities are represented by four-pole parameters as

$$\begin{bmatrix} p_3 \\ v_3 \end{bmatrix} = \mathbf{T}_d \begin{bmatrix} p_6 \\ v_6 \end{bmatrix}, \tag{15}$$

where junction points 3 and 6 are the input and the output of "element d," respectively.

Conditions of pressure equilibrium and conservation of volume velocity at the first junction point yield

$$p_1 = p_2 = p_3 = p_4, \tag{16}$$

$$v_1 = v_2 + v_3 + v_4, \tag{17}$$

where $p_1$, $p_2$, $p_3$ and $p_4$ are the sound pressures, and $v_1$, $v_2$, $v_3$ and $v_4$ are the volume velocities. Furthermore, at the second junction point,

$$p_5 = p_6 = p_7 = p_8, \tag{18}$$

$$\nu_5 + \nu_6 = \nu_7 + \nu_8, \tag{19}$$

where $p_5$, $p_6$, $p_7$ and $p_8$ are the sound pressures, and $\nu_5$, $\nu_6$, $\nu_7$ and $\nu_8$ are the volume velocities.

At junction point 0, the sound pressure and the volume velocity from Eqn. (11) give

$$p_0 = A_a p_1 + B_a \nu_1, \tag{20}$$

$$\nu_0 = C_a p_1 + D_a \nu_1. \tag{21}$$

The transfer matrix corresponding to resonators connected to the main duct can be expressed as the product of the transfer matrices of the elements $b_1$, $b_2$, $e_1$ and $e_2$ as

$$\mathbf{T}_{hr_1} = \mathbf{T}_{b_1}\mathbf{T}_{e_1}, \tag{22}$$

and

$$\mathbf{T}_{hr_2} = \mathbf{T}_{b_2}\mathbf{T}_{e_2}. \tag{23}$$

Finally,

$$\mathbf{T}_{hr} = \begin{bmatrix} A_{hr} & B_{hr} \\ C_{hr} & D_{hr} \end{bmatrix}. \tag{24}$$

Thus, the sound pressure and volume velocity at junction point 2 (the upper part of the first resonator) may be obtained from the sound pressure and volume velocity at junction point 10 (the end of the first resonator).

$$p_2 = A_{hr_1} p_{10}, \tag{25}$$

$$\nu_2 = C_{hr_1} p_{10}. \tag{26}$$

Junction points 4 and 5 are the input and the output of the side branch duct modified with an expansion chamber. From Eqn. (12) the sound pressure and volume velocity at the junction point 4 can be written as

$$p_4 = A_c p_5 + B_c \nu_5, \tag{27}$$

$$\nu_4 = C_c p_5 + D_c \nu_5. \tag{28}$$

Examining "element d," the pressure and velocity relationships between junction points 3 and 6 are

$$p_3 = A_d p_6 + B_d \nu_6, \tag{29}$$

$$\nu_3 = C_d p_6 + D_d \nu_6. \tag{30}$$

Similarly, the pressure and velocity relationships between junction point 7 (the upper of the second resonator) and junction point 11 (the end of the second resonator) are

$$p_7 = A_{hr_2} p_{11}, \tag{31}$$

$$\nu_7 = C_{hr_2} p_{11}. \tag{32}$$

Substituting $p_7 = p_8$ into Eqn. (31) yields

$$p_8 = A_{hr_2} p_{11}. \tag{33}$$

The sound pressure at the end of the second resonator can be written as

$$p_{11} = \frac{p_8}{A_{hr_2}}. \tag{34}$$

The volume velocity $\nu_7$ can be expressed in terms of the sound pressure $p_8$ as

$$\nu_7 = \frac{C_{hr_2}}{A_{hr_2}} p_8. \tag{35}$$

Junction points 8 and 9 correspond to the input and output of "element f," respectively. Then,

$$p_8 = A_f p_9 + B_f \nu_9, \tag{36}$$

$$\nu_8 = C_f p_9 + D_f \nu_9, \tag{37}$$

Eqns. (28) and (29) give

$$A_d p_6 + B_d \nu_6 = A_c p_5 + B_c \nu_5. \tag{38}$$

Substituting $p_5 = p_6 = p_8$ into Eqn. (38) and rearranging results in

$$A_d p_8 - A_c p_8 + B_d \nu_6 = B_c \nu_5. \tag{39}$$

Thus, the volume velocity, $\nu_5$, at junction point 5 is

$$\nu_5 = \frac{A_d - A_c}{B_c} p_8 + \frac{B_d}{B_c} \nu_6. \tag{40}$$

Substituting Eqn. (40) into Eqn. (19) results in

$$\frac{A_d - A_c}{B_c} p_8 + \frac{B_d}{B_c} \nu_6 + \nu_6 = \frac{C_{hr_2}}{A_{hr_2}} p_8 + \nu_8, \tag{41}$$

giving

$$\nu_6 = \left( \frac{B_c C_{hr_2} - A_{hr_2}(A_d - A_c)}{(B_c + B_d) A_{hr_2}} \right) p_8 + \left( \frac{B_c}{B_c + B_d} \right) \nu_8. \tag{42}$$

Thus, Eqns. (25) and (29) give

$$A_{hr_1} p_{10} = A_d p_6 + B_d \nu_6 \tag{43}$$

Equation (43) may be rearranged further by substituting $p_8 = p_6$.

Thus, the sound pressure at the end of the first resonator is

$$p_{10} = \frac{A_d}{A_{hr_1}} p_8 + \frac{B_d}{A_{hr_1}} \nu_6. \tag{44}$$

Substituting Eqns. (26) and (28) into Eqn. (30) yields

$$v_1 = C_{hr_1} p_{10} + C_d p_8 + D_d v_6 + C_c p_5 + D_c v_5. \quad (45)$$

Substituting $v_5$ from Eqn. (40), $v_6$ from Eqn. (42) and $p_{10}$ from Eqn. (44) into Eqn. (45) results in

$$\begin{aligned} v_1 = \Bigg( & \frac{A_d C_{hr_1}}{A_{hr_1}} + C_d + C_c \\ & + \frac{B_d C_{hr_1}}{A_{hr_1}} \frac{B_c C_{hr_2} - A_{hr_2}(A_d - A_c)}{(B_c + B_d) A_{hr_2}} \\ & + \frac{D_d (B_c C_{hr_2} - A_{hr_2}(A_d - A_c))}{(B_c + B_d) A_{hr_2}} + \frac{D_c (A_d - A_c)}{B_c} \\ & + \frac{D_c B_d}{B_c} \frac{(B_c C_{hr_2} - A_{hr_2}(A_d - A_c))}{(B_c + B_d) A_{hr_2}} \Bigg) p_8 \\ & + \frac{B_d C_{hr_1} B_c}{(B_c + B_d) A_{hr_1}} + \frac{D_b B_c}{(B_c + B_d)} + \frac{B_d D_c B_c}{(B_c + B_d) B_c} \Bigg) v_8. \end{aligned} \quad (46)$$

Then,

$$\begin{aligned} C_{18} = & \frac{A_d C_{hr_1}}{A_{hr_1}} + C_d + C_c + \frac{B_d C_{hr_1}}{A_{hr_1}} \frac{B_c C_{hr_2} - A_{hr_2}(A_d - A_c)}{(B_c + B_d) A_{hr_2}} \\ & + \frac{D_d (B_c C_{hr_2} - A_{hr_2}(A_d - A_c))}{(B_c + B_d) A_{hr_2}} + \frac{D_c (A_d - A_c)}{B_c} \\ & + \frac{D_c B_d}{B_c} \frac{(B_c C_{hr_2} - A_{hr_2}(A_d - A_c))}{(B_c + B_d) A_{hr_2}}, \end{aligned} \quad (47)$$

and

$$D_{18} = \frac{B_d C_{hr_1} B_c}{(B_c + B_d) A_{hr_1}} + \frac{D_b B_c}{(B_c + B_d)} + \frac{B_d D_c B_c}{(B_c + B_d) B_c}, \quad (48)$$

are obtained, where $C_{18}$ and $D_{18}$ are two elements of the transfer matrix $\mathbf{T}_{18}$ as defined by Eqn. (10). These expressions for the elements $C_{18}$ and $D_{18}$ imply certain physical significance. $C_{18}$ is the ratio of the velocity at the inlet to the outlet pressure for the hypothetical case of the outlet being rigidly fixed ($Z_f \rightarrow \infty$), and $D_{18}$ is the ratio of the velocity at the inlet to the velocity at the outlet for the hypothetical case of the outlet being totally open or unconstrained ($Z_f \rightarrow 0$)[22].

Equilibrium of volume velocity at the second junction point yields

$$\begin{aligned} v_5 = v_7 + v_8 - v_6 = & \frac{C_{hr_2}}{A_{hr_2}} p_8 + v_8 \\ & - \left( \frac{B_c C_{hr_2} - (A_d - A_c) A_{hr_2}}{(B_c + B_d) A_{hr_2}} \right) p_8 + \left( \frac{B_c}{B_c + B_d} \right) v_8. \end{aligned} \quad (49)$$

Substituting $p_1 = p_4$ and $p_5 = p_8$ into Eqn. (27) results in

$$p_1 = A_c p_8 + B_c v_5. \quad (50)$$

By substituting $v_5$ from Eqn. (49) into the Eqn. (50), the sound pressure at the output of "element a" is found, in terms of $p_8$ and $v_8$, as

$$\begin{aligned} p_1 = & A_c p_8 + \frac{B_c C_{hr_2}}{A_{hr_2}} p_8 + B_c v_8 \\ & - \frac{B_c^2 C_{hr_2} - B_c (A_d - A_c) A_{hr_2}}{(B_c + B_d) A_{hr_2}} p_8 - \frac{B_c^2}{B_c + B_d} v_8. \end{aligned} \quad (51)$$

Then,

$$A_{18} = A_c + \frac{B_c C_{hr_2}}{A_{hr_2}} - \frac{B_c^2 C_{hr_2} - B_c (A_d - A_c) A_{hr_2}}{(B_c + B_d) A_{hr_2}} \quad (52)$$

and

$$B_{18} = B_c - \frac{B_c^2}{B_c + B_d} = \frac{B_c B_d}{B_c + B_d}, \quad (53)$$

are obtained, where $A_{18}$ and $B_{18}$ are the other two elements of the transfer matrix $T_{18}$ as defined by Eqn. (10). The elements $A_{18}$ and $B_{18}$ have individual physical meaning. $A_{18}$ is the ratio between the inlet pressure and the outlet pressure for the hypothetical case of the outlet being rigidly fixed ($Z_f \rightarrow \infty$), and $B_{18}$ is the ratio of the inlet pressure to the velocity at the outlet for the hypothetical case of the outlet being totally open or unconstrained ($Z_f \rightarrow 0$)[22]. $Z_a$ and $Z_f$ are the impedances of "element a" and "element f," respectively. $A_{18}$, $B_{18}$, $C_{18}$ and $D_{18}$ are frequency-dependent complex quantities embodying the acoustical properties of the system. These parameters are depending on the system geometry, and they are not affected by connections to elements upstream or downstream, as long as the system elements can be assumed to be linear and passive[16].

On the other hand, in this study, the characteristic impedances are assumed to be equal at the inlet and the outlet: $Z_a = Z_f = Z$. The transfer matrix of the system shown in Fig. 1 is obtained as $\mathbf{T}_{18}$.

Transmission loss involves neither the source nor the radiation impedance. It is an invariant property of the

element. Since it is independent of the terminations, TL finds favor with researchers who are interested in finding the acoustic transmission behavior of an element or set of elements in the context of isolated terminations[22].

Finally, the TL of the system can be expressed as

$$TL = 20Log_{10}\left|\frac{1}{2}\left(A_{18}+\frac{B_{18}}{Z}+ZC_{18}+D_{18}\right)\right|. \quad (54)$$

## 3 RESULTS AND DISCUSSION

This section is devoted to the numerical evaluations of the expressions given in the preceding section and the finite element models. In order to determine the multi-dimensional effects on the acoustic performance of the system, a finite element method model was developed using the MSc. Actran software package.

In each of the finite element analysis applications, we first built a solid model of the system using a 3D CAD program, Unigraphics Nx-4. Then, the solid model was exported to MSc.Patran in parasolid format. This solid model consists of the air in the pipe system, which is called the cavity in this paper. The cavity is meshed using first order tetrahedral solid elements. In numerical acoustic analysis, the mesh size must be smaller than one sixth of the wavelength (mesh size $<\lambda/6$). The frequency range examined in this work is 0–3000 Hz. The minimum wavelength is $\lambda=0.113$ m, and the mesh size used in our numerical analysis is 0.012 m. After meshing the cavity using solid elements, the input and output faces of the cavity were meshed with first order triangular elements. Two local coordinates with the same x-direction were assigned to these new faces, to give the input and output. Our goal was to be able to read the input and output sound power values after the analysis. A sound pressure value of 1 Pa was set for the nodes on the input face of the cavity. Then, we created a material with the default values of air. The density was 1.225 kg/m$^3$, and the sound speed was 340 m/s. Using the default values in the software, the damping effect of air was not taken into account and was also not considered in our analytical model. We processed the output data in order to obtain the TL of the system. The results were then compared with the analytical analyses.

The transfer matrix method based on the plane wave propagation model is valid when the influence of higher order modes can be neglected.

In view of the many possibilities and variations in terms of the dimensions and number of acoustical elements, our present study focuses on structures with certain discrete duct lengths and diameters.

The duct lengths are significant to reach the expected frequency response of the system. The bandwidth of the modified HQ tube developed by Selamet and Easwaran[8] and later used by Trochon[17] is dependent on the center frequency of the filter. This is related to the fixed ratios of the constituent pipe lengths.

The resonance of a duct that is open at both ends occurs when the frequency is

$$f=\frac{c}{2l_{hq}}p, \quad p=1,2,3,\ldots \quad (55)$$

where c is the speed of sound. Setting the design length of the side branch duct, $l_{hq}$, to 200 mm, the first, second and third resonance frequencies of the duct are approximately 850, 1700 and 2,550 Hz, respectively.

The resonance frequencies of the system consisting of a side branch duct connected to the main duct can be estimated as

$$f=\frac{c}{2(l_{hq}-l_d)}(2p+1), \quad p=0,1,2,3,\ldots \quad (56)$$

and

$$f=\frac{c}{(l_{hq}+l_d)}p, \quad p=1,2,3,\ldots \quad (57)$$

Setting the lengths of the side branch duct, $l_{hq}$, and the main duct, $l_d$, to 200 mm and 100 mm, the resonance frequencies of the system can be calculated as approximately 1125, 1700 and 2,250 Hz, respectively. These parameters remain constant throughout our analysis. At these frequencies, the theoretical transmission loss of the system becomes infinite.

The starting configuration of the system was suggested based upon results found in the literature[7,8,17,19] and was consistent with our initial resonance calculations.

Figures 2–4 show the effects of the diameters of the main duct and the side branch duct on the acoustic attenuation performance of the system, for geometries ($h_{md}=18$ mm, $h_{hq}=3$ mm), ($h_{md}=36$ mm, $h_{hq}=18$ mm) and ($h_{md}=36$ mm, $h_{hq}=36$ mm), respectively. In these three cases, the length of the main duct and the length of the side branch duct are taken into account as $l_d=100$ mm and $l_{hq}=200$ mm. In our figures, the analytical and numerical results are shown together. There are three peaks in the TL curves across several related frequency bandwidths. For these cases, the initial resonance calculations show that the resonance frequencies are 850 Hz from Eqn. (55) for $l_{hq}=200$ mm, 1700 Hz from Eqns. (55)–(57) and 2550 Hz from Eqn. (55). From the figures, the effect of the diameters of the main duct and the side branch duct on the TL is very clear. For small diameter ratios of the main duct and the side branch duct, the TL

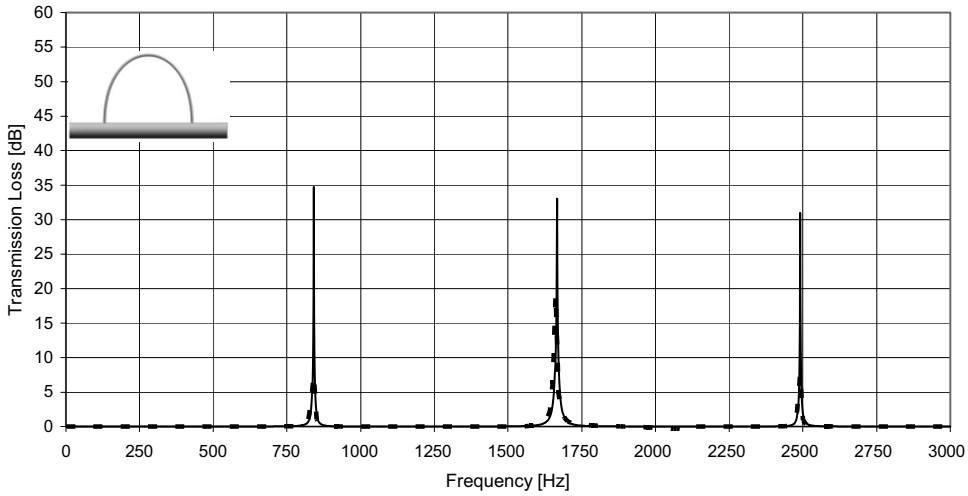


*Fig. 2—TL of the system consisting of a side branch duct connected to the main duct. $h_{md}$=18 mm, $h_{hq}$ =3 mm, $l_d$=100 mm, $l_{hq}$=200 mm. – – – Numerical, — Analytical.*

frequency bandwidths are narrow, but we note that the greater the ratio of the diameters, the wider the TL frequency bandwidth. Furthermore, our comparisons show that given the small diameter ratios, our analytical and numerical results are in good agreement. For greater diameter ratios, our results are in satisfactory agreement in the related frequency bandwidth. We note again that the transfer matrix method can only be used for plane-wave conditions.

The resonance frequencies of the quarter wave resonator can be calculated as

$$f = \frac{c}{4l_{hr}}(2p+1), \quad p = 0,1,2,3,\ldots \tag{58}$$

Figures 5 and 6 indicate the TL treatment of the system consisting of a side branch duct and one and two quarter wave resonators, separately, both connected to the main duct, for geometries, $h_{md}$=36 mm, $h_{hq}$ =18 mm, $l_{hr}$=50 mm, $l_d$=100 mm and $l_{hq}$=200 mm. For these cases, the initial calculations indicate that the resonance frequencies are 850 Hz from Eqn. (55) for $l_{hq}$=200 mm, 1700 Hz from Eqns. (55)–(57) and 2550 Hz from Eqn. (55). Furthermore, setting the length of the quarter wave resonator, $l_{hr}$, to 50 mm, the first resonance frequency of the quarter wave resonators can be calculated as approximately 1700 Hz. In the figures, the analytical and numerical results are shown together. There are three peaks in the TL curves in the related frequency bandwidth. Both analytical and numerical TL curves reveal the same characteristics, and the results are in agreement. The effect of the attachment of a one quarter wave resonator is analyzed in Fig. 5. Comparison of Fig. 3 and Fig. 5 shows that the quarter wave resonator eliminates any significant changes in TL levels. The effect of

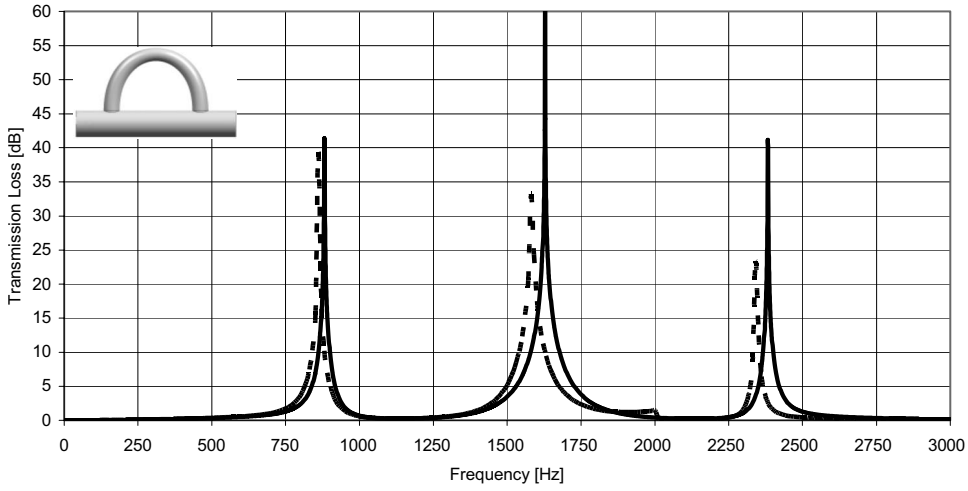


*Fig. 3—TL of the system consisting of a side branch duct connected to the main duct. In this case, while $h_{md}$ and $h_{hq}$ increase, $l_d$, and $l_{hq}$ are kept constant according to Fig. 2. $h_{md}$=36 mm, $h_{hq}$=18 mm, $l_d$=100 mm, $l_{hq}$=200 mm. – – – Numerical, — Analytical.*

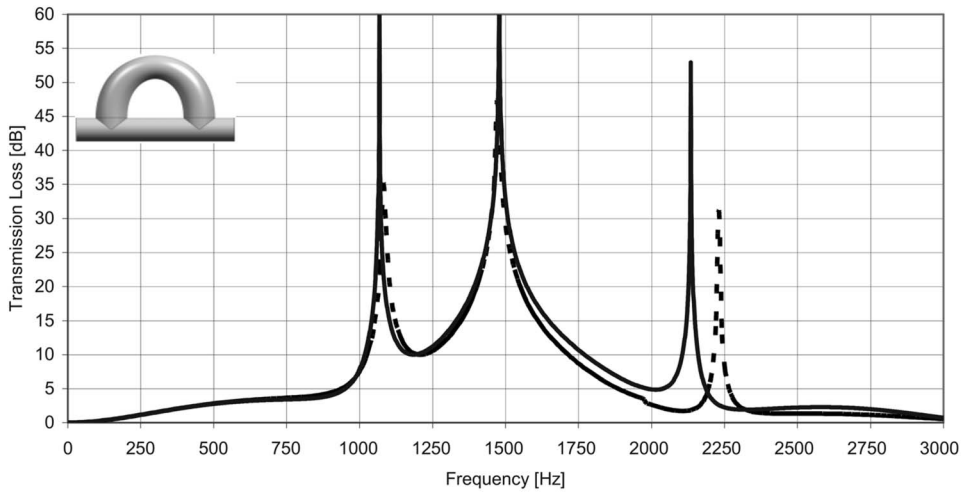


*Fig. 4—TL of the system consisting of a side branch duct connected to the main duct. In this case, while only $h_{hq}$ increases, $h_{md}$, $l_d$, and $l_{hq}$ are kept constant according to Fig. 3. $h_{md}$=36 mm, $h_{hq}$ =36 mm, $l_d$=100 mm, $l_{hq}$=200 mm. – – – Numerical, — Analytical.*

the attachment of one more quarter wave resonator is analyzed in Fig. 6. Comparison of Fig. 5 and Fig. 6 indicates that the three TL peaks move approximately 50 Hz downwards, and significant changes in TL levels and frequency bandwidths are not observed.

In order to indicate the effects of the diameters of two quarter wave resonators on the TL characteristic of the system, TL behaviors are compared in Fig. 7. This figure shows our analytical results. The TL frequency bandwidths tend to decrease in the side branch duct and the resonator diameters increase. A minimum of 10 dB of TL between 1050–1600 Hz can be obtained with the geometry shown in the figure. In addition, we note that with a greater diameter of the side branch duct, the first TL peak moves approximately 100 Hz upwards, and the third TL peak moves approximately 100 Hz downwards at the same time.

Figure 8 shows the effect of a side branch duct modified with an expansion chamber connected to the main duct in terms of the acoustic attenuation performance of the system. The illustration shows results for geometries $h_{md}$=18 mm, $h_{hq}$=3 mm, $h_{ec}$=6 mm, $l_d$ =100 mm, $l_{ec}$=67 mm and $l_{hq}$=200 mm. Both analytical and numerical TL curves show the same trends and the results are in good agreement. Comparison of Fig. 2 and Fig. 8 shows that the first TL peak moves approximately 300 Hz downwards, the second peak moves approximately 300 Hz upwards, and there is no change in the

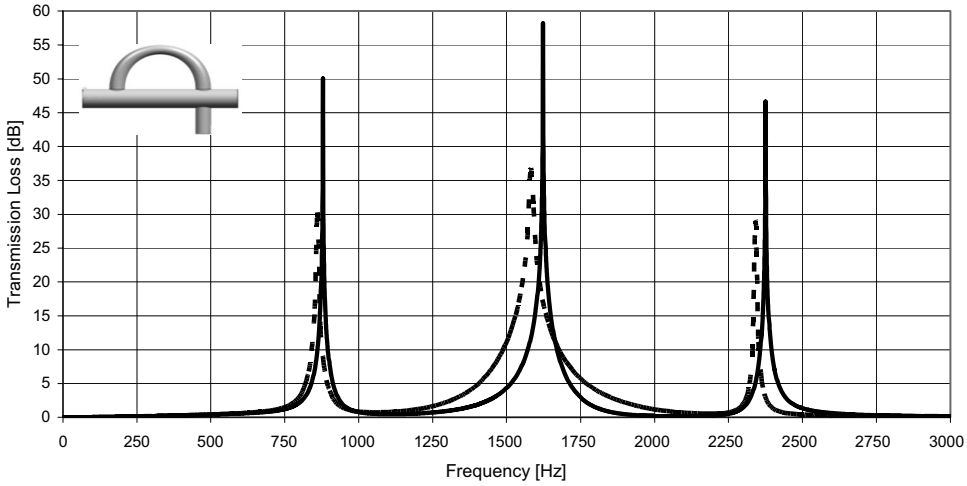


*Fig. 5—TL of the system consisting of a side branch duct and a quarter wave resonator connected to the main duct. In this case, $h_{md}$, $h_{hq}$, $l_d$, and $l_{hq}$ are kept constant according to Fig. 3, and a quarter wave resonator is connected to the main duct. $h_{md}$=36 mm, $h_{hq}$=18 mm, $l_{hr}$=50 mm, $l_d$=100 mm, $l_{hq}$=200 mm. – – – Numerical, — Analytical.*

_ _ _ Numerical, ___ Analytical.

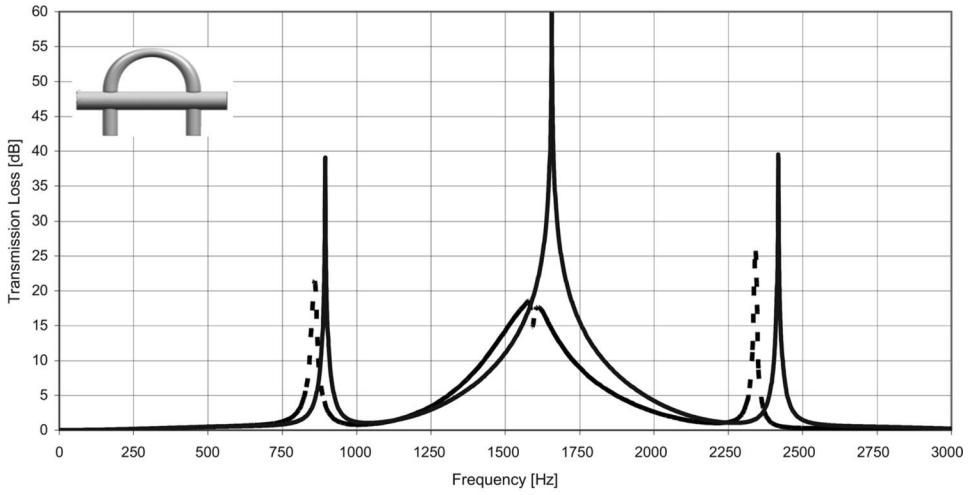


*Fig. 6—TL of the system consisting of a side branch duct and two quarter wave resonators connected to the main duct. In this case, $h_{md}$, $h_{hq}$, $l_d$, and $l_{hq}$ are kept constant according to Fig. 3, and two quarter wave resonators are connected to the main duct. $h_{md}$=36 mm, $h_{hq}$=18 mm, $l_{hr}$=50 mm, $l_d$=100 mm, $l_{hq}$=200 mm. – – – Numerical, — Analytical.*

frequency of the third peak. In this case, there is a new peak at 3000 Hz. The TL levels are higher than the first case.

Comparison of Fig. 8 and Fig. 9 demonstrates that when two quarter wave resonators are connected to the main duct a new resonance peak appears at approximately 1700 Hz. Calculations indicate that the new resonance peak results from the quarter wave resonators given $h_{hr}$=3 mm, $l_{hr}$=50 mm.

Figures 9 and 10 show the TL behaviors of the system consisting of two quarter wave resonators and a side branch duct modified with an expansion chamber and all connected to the main duct, for geometries ($h_{md}$=18 mm, $h_{hq}$=3 mm, $h_{ec}$=6 mm, $h_{hr1,hr2}$=3 mm) and ($h_{md}$=18 mm, $h_{hq}$=9 mm, $h_{ec}$=18 mm, $h_{hr1,hr2}$=9 mm), respectively. In these two cases, the dimensions that are held constant are $l_{hr}$=50 mm, $l_d$=100 mm, $l_{ec}$=67 mm and $l_{hq}$=200 mm. In the figures, both the analytical and numerical results are shown together. Comparisons show that for small diameters, analytical and numerical results are in good agreement; in addition, for the larger diameters, results are in satisfactory agreement across related frequency bandwidths because of the limitations of the plane wave approach. Specifically, there

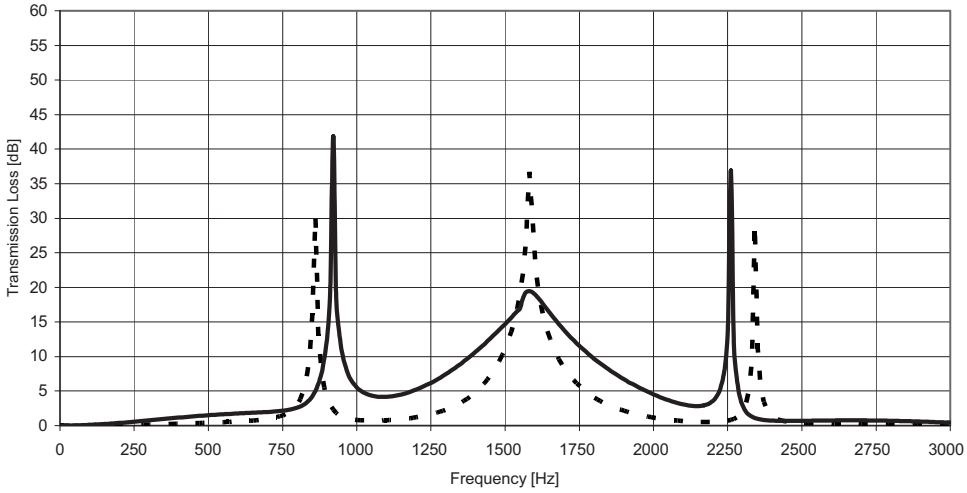


*Fig. 7—TL of the system consisting of a side branch duct and two quarter wave resonators connected to the main duct. $h_{md}$=36 mm, $l_{hr}$=50 mm, $l_d$=100 mm, $l_{hq}$=200 mm. – – – $h_{hr}$=18 mm, — $h_{hr}$=27 mm.*

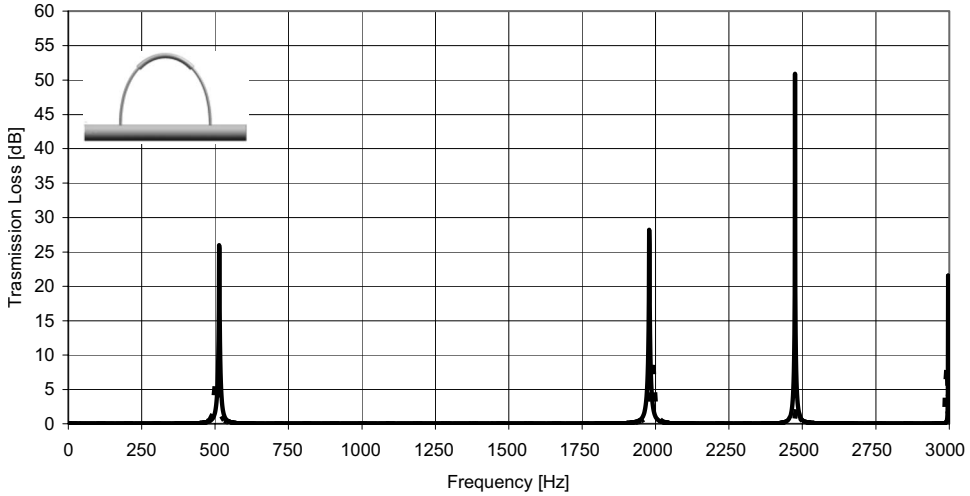


*Fig. 8—TL of the system consisting of a side branch duct modified with an expansion chamber connected to main duct. In this case, $h_{md}$, $h_{hq}$, $l_d$, and $l_{hq}$ are kept constant according to Fig. 2, and an expansion chamber is located at the side brunch duct. $h_{md}$=18 mm, $h_{hq}$=3 mm, $h_{ec}$=6 mm, $l_d$ =100 mm, $l_{ec}$=67 mm, $l_{hq}$=200 mm. – – – Numerical, — Analytical.*

are five peaks in the TL curves for a related frequency bandwidth given the geometries taken into consideration. Comparisons between Fig. 9 and Fig. 10 show that for small diameters of the resonators and the side branch duct, the TL frequency bandwidths are narrow, but we note that the greater the diameters, the wider the TL frequency bandwidths. Additionally, there are no significant changes in the frequencies of the first three peaks, but the fourth TL peak moves approximately 100 Hz downwards. Furthermore, the TL levels are higher.

In this case, we analyze the effects of the position and the length of the expansion chamber on the TL behavior of a system consisting of two quarter wave resonators and a side branch duct modified with an expansion chamber, all connected to the main duct. Figures 11 and 12 compare the TL behaviors of the system in order to show the effects of the geometric parameters on the TL characteristic, for geometries ($l_{ec}$=40 mm, $l_{ec}$=60 mm, $l_{ec}$=80 mm) and ($l_{c1}$ =20 mm, $l_{c1}$=40 mm, $l_{c1}$=60 mm, $l_{c1}$=80 mm, $l_{c1}$ =100 mm), respectively. In these two cases, the dimensions that are held constant are $h_{md}$=18 mm, $h_{hq}$ =9 mm, $h_{ec}$=18 mm, $h_{hr1,hr2}$=9 mm, $l_{hr}$=50 mm, $l_d$ =100 mm, $l_{ec}$=67 mm and $l_{hq}$=200 mm. The major effect of the length of the expansion chamber lies in shifting the TL peak frequencies of the system. With the change of the position of the expansion chamber, no systematic or noticeable change occurs in TL levels.

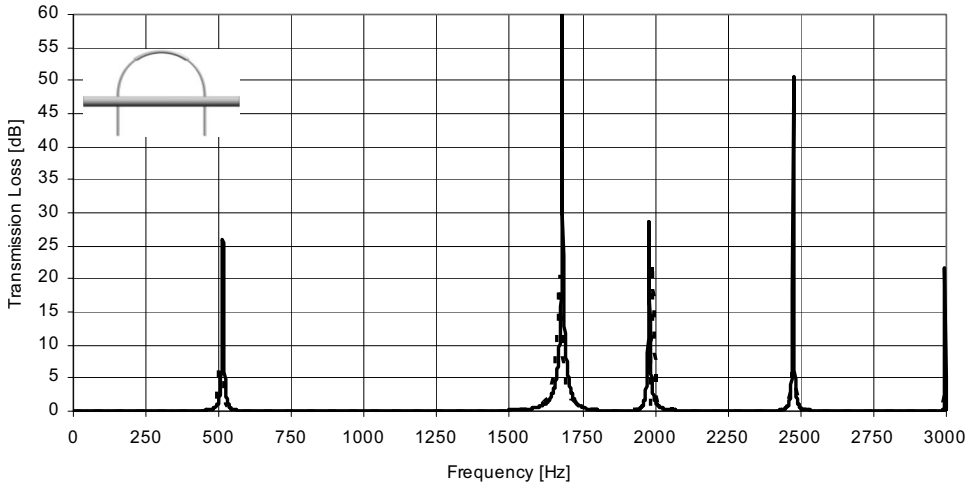


*Fig. 9—TL of the system consisting of a side branch duct modified with an expansion chamber and two quarter wave resonators connected to the main duct. $h_{md}$=18 mm, $h_{hq}$=3 mm, $h_{ec}$=6 mm, $h_{hr1,hr2}$=3 mm, $l_{hr}$=50 mm, $l_d$=100 mm, $l_{ec}$=67 mm, $l_{hq}$=200 mm. – – – Numerical, — Analytical.*

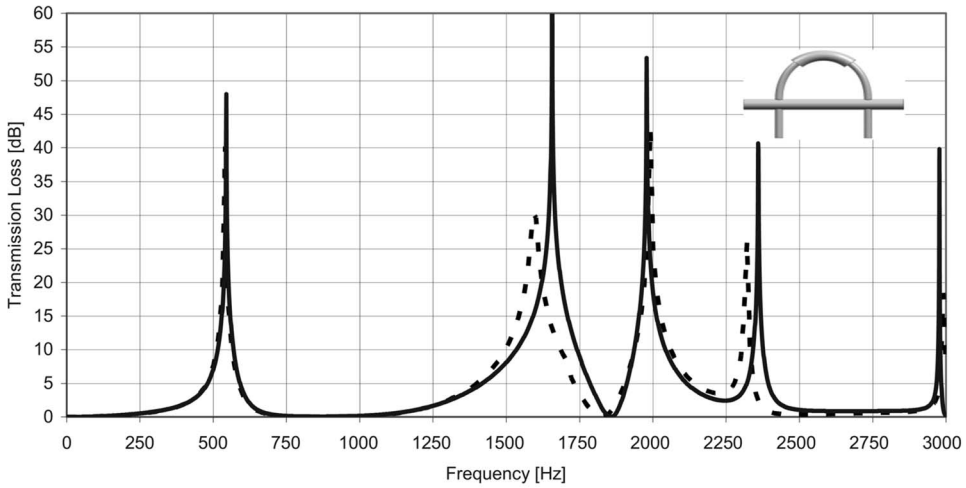


*Fig. 10—TL of the system consisting of a side branch duct modified with an expansion chamber and two quarter wave resonators connected to the main duct. $h_{md}=18$ mm, $h_{hq}=9$ mm, $h_{ec}=18$ mm, $h_{hr1,hr2}=9$ mm, $l_{hr}=50$ mm, $l_d=100$ mm, $l_{ec}=67$ mm, $l_{hq}=200$ mm. – – – Numerical, — Analytical.*

However, the major effect of the position of the expansion chamber to the TL curve is to shift the resonant frequencies.

The resonance frequencies of the Helmholtz resonators were based on the volume of the cavity and the radius of the opening, which after some rearrangement is given by

$$f=\frac{c}{2\pi}\sqrt{\frac{h_n^2}{h_{hr}^2 l_{hr} l_n}}. \tag{59}$$

In the next case, we analyze the diameter and length of the neck on TL behavior of the system consisting of two Helmholtz resonators connected to main duct and a side branch duct. Figures 13 and 14 present the TL behaviors of the system for geometries ($h_{md}$=36 mm, $h_{hq}$=36 mm, $l_d$=100 mm, $l_{hq}$=200 mm, $h_{n1,n2}$=12 mm, $h_{hr1,hr2}$=36 mm, $l_{n1,n2}$=15 mm, $l_{hr1,hr2}$=45 mm) and ($h_{md}$=18 mm, $h_{hq}$=18 mm, $l_d$=100 mm, $l_{hq}$=200 mm, $h_{ec}$=24 mm, $l_{ec}$=67 mm, $h_{n1,n2}$=12 mm, $h_{hr1,hr2}$=36 mm, $l_{n1,n2}$=12 mm, $l_{hr1,hr2}$=50 mm), respectively. For the case in Fig. 13, initial calculations indicate that the resonance frequencies are 690 Hz from Eqn. (59), 1125 Hz from Eqn. (55), 1700 Hz from Eqns. (56) and (57) and 2250 Hz from Eqn. (55). For the case in Fig. 14, calculations show that the resonance frequencies are 730 Hz from Eqn. (59), 1125 Hz from Eqn. (55),

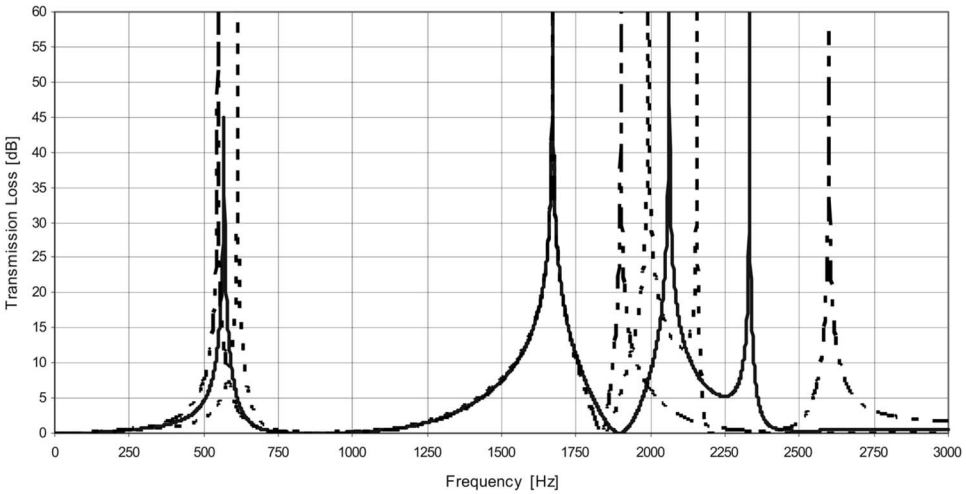


*Fig. 11—TL of the system consisting of a side branch duct modified with an expansion chamber and two quarter wave resonators connected to the main duct. $h_{md}=18$ mm, $h_{hq}=9$ mm, $h_{ec}=18$ mm, $h_{hr1,hr2}=9$ mm, $l_{hr}=50$ mm, $l_d=100$ mm, $l_{hq}=200$ mm. – – – $l_{ec}=40$ mm, — $l_{ec}=60$ mm, — – — $l_{ec}=80$ mm.*

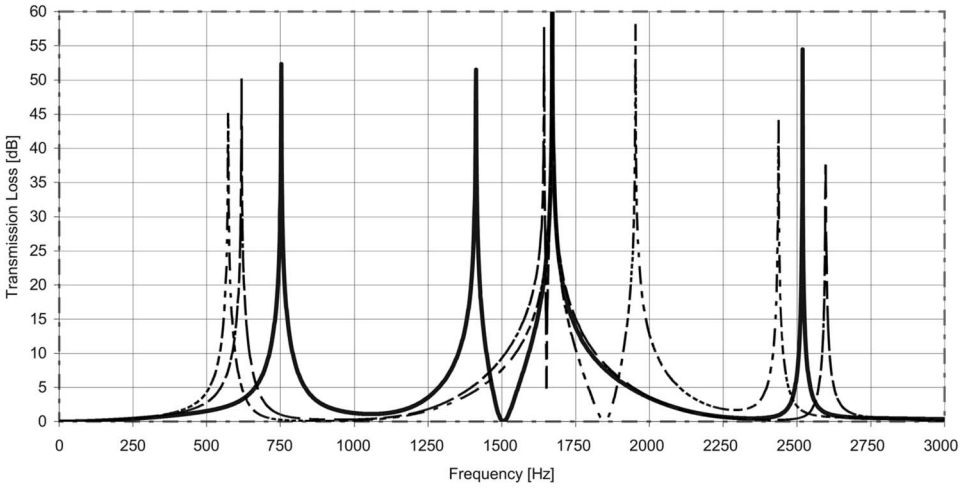


*Fig. 12—TL of the system consisting of a side branch duct modified with an expansion chamber and two quarter wave resonators connected to the main duct. $h_{md}=18$ mm, $h_{hq}=9$ mm, $h_{ec}=18$ mm, $h_{hr1,hr2}=9$ mm, $l_{hr}=50$ mm, $l_d=100$ mm, $l_{ec}=67$ mm, $l_{hq}=200$ mm. — $l_{c1}=20$ mm, — – $l_{c1}=40$ mm, — — — — $l_{c1}=60$ mm, - - - $l_{c1}=80$ mm, – – – $l_{c1}=100$ mm.*

1700 Hz from Eqns. (56) and (57) and 2250 Hz from Eqn. (55). These configurations exhibit frequency bands where the transmission loss is high. The width of the attenuation bands near resonances is considerable, which may prove to be useful for noise control. Comparison of Fig. 4 and Fig. 13 shows the effect of the Helmholtz resonators connected to main duct. They carry a new TL peak into the related frequency range. The contributions of the necks are also positive in terms of the frequency behavior of the system.

Figures 15–20 illustrate analytical results from parametric studies on the TL behaviors of the system.

The effect of the length of the side branch duct is investigated and shown in Fig. 15, for geometries $l_{hq}=198$ mm, $l_{hq}=204$ mm, $l_{hq}=210$ mm, $l_{hq}=216$ mm and $l_{hq}=222$ mm, respectively. In these cases, the dimensions that are held constant are $h_{md}=36$ mm, $h_{hq}=36$ mm, $l_d=100$ mm, $h_{n1,n2}=12$ mm, $h_{hr1,hr2}=36$ mm, $l_{n1,n2}=15$ mm and $l_{hr1,hr2}=45$ mm. There is no significant change in the frequency and the level of the first peak, but the other peaks shift downwards. The considerable contribution of the length of the side branch duct is seen in the third TL peak. As indicated in the initial resonance calculations from Eqn. (59), the resonance

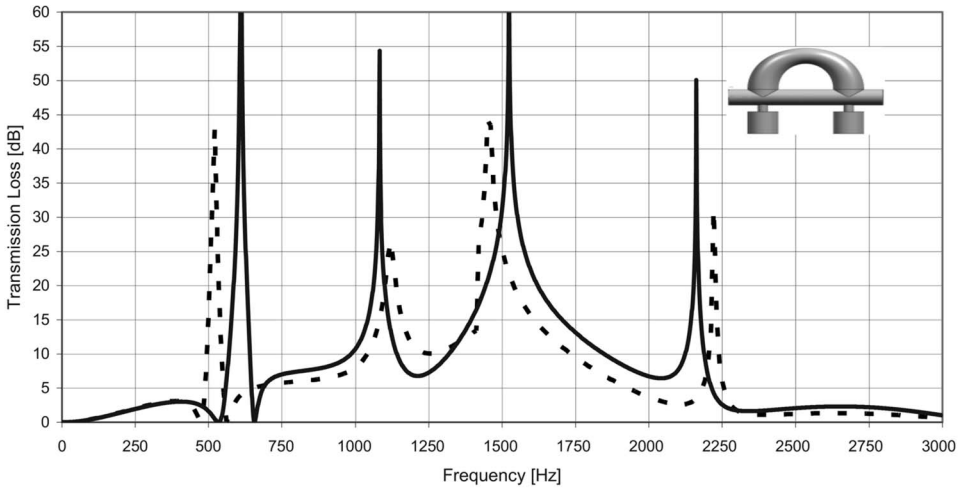


*Fig. 13—TL of the system consisting of a side branch duct and two Helmholtz resonators connected to the main duct. In this case, $h_{md}$, $h_{hq}$, $l_d$, and $l_{hq}$ are kept constant according to Fig. 3, and two Helmholtz resonators are connected to the main duct. $h_{md}=36$ mm, $h_{hq}=36$ mm, $l_d=100$ mm, $l_{hq}=200$ mm, $h_{n1,n2}=12$ mm, $h_{hr1,hr2}=36$ mm, $l_{n1,n2}=15$ mm, $l_{hr1,hr2}=45$ mm. – – – Numerical, — Analytical.*

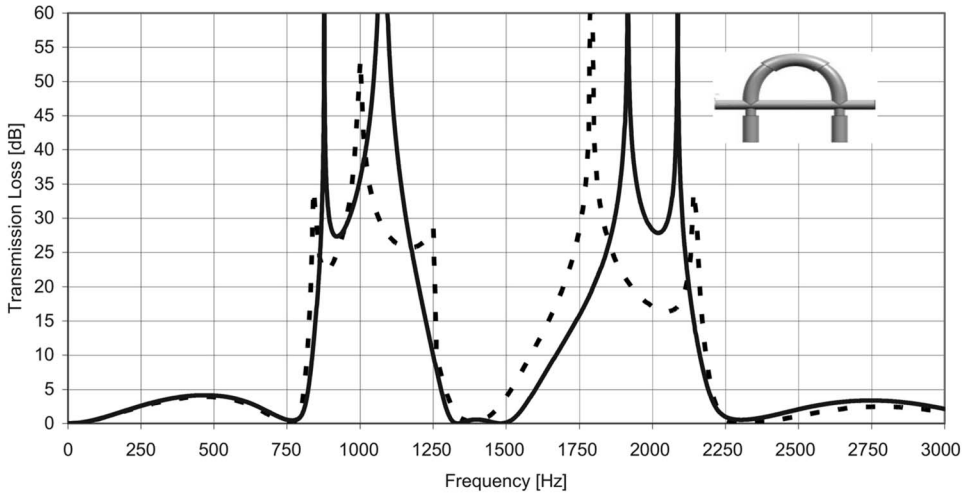


*Fig. 14—TL of the system consisting of a side branch duct modified with an expansion chamber and two Helmholtz resonators connected to the main duct. $h_{md}=18$ mm, $h_{hq}=18$ mm, $l_d=100$ mm, $l_{hq}=200$ mm, $h_{ec}=24$ mm, $l_{ec}=67$ mm, $h_{n1,n2}=12$ mm, $h_{hr1,hr2}=36$ mm, $l_{n1,n2}=12$ mm, $l_{hr1,hr2}=50$ mm. – – – Numerical, — Analytical.*

frequencies change between 1730 Hz for $l_{hq}=198$ mm and 1390 Hz for $l_{hq}=222$ mm; the second and the third TL peaks are affected mainly by the length of the side branch duct. TL levels increase in the low frequency range, whereas the levels decrease at high frequencies, as shown in the figure. At higher frequencies, the collapse of the TL consistent with the length of the side branch duct is evident.

In the next case, we analyze the length of the neck, as shown in Fig. 16, for geometries $l_{n1,n2}=5$ mm, $l_{n1,n2}=10$ mm, $l_{n1,n2}=15$ mm, $l_{n1,n2}=20$ mm and $l_{n1,n2}=25$ mm. In these cases, the dimensions that are held constant are $h_{md}=36$ mm, $h_{hq}=36$ mm, $l_d=100$ mm, $h_{n1,n2}=12$ mm, $h_{hr1,hr2}=36$ mm, $l_{hr1,hr2}=45$ mm and $l_{hq}=200$ mm. The main effects of the length of the neck are especially evident in the first TL peak. Comparison of the results shows that the longer the length, the lower the frequency of the first TL peak. There is no significant change in the TL levels, especially for the first TL peak. From Eqn. (59), the resonance frequencies vary between 1200 Hz for $l_n=5$ mm and 530 Hz for $l_n=25$ mm; the first TL peak is affected mainly by the length of the neck. The frequency bandwidth of the first TL peak narrows while the resonance frequencies decrease.

The contribution of the lengths of the Helmholtz resonators is studied in Fig. 17 for geometries $l_{hr1,hr2}$

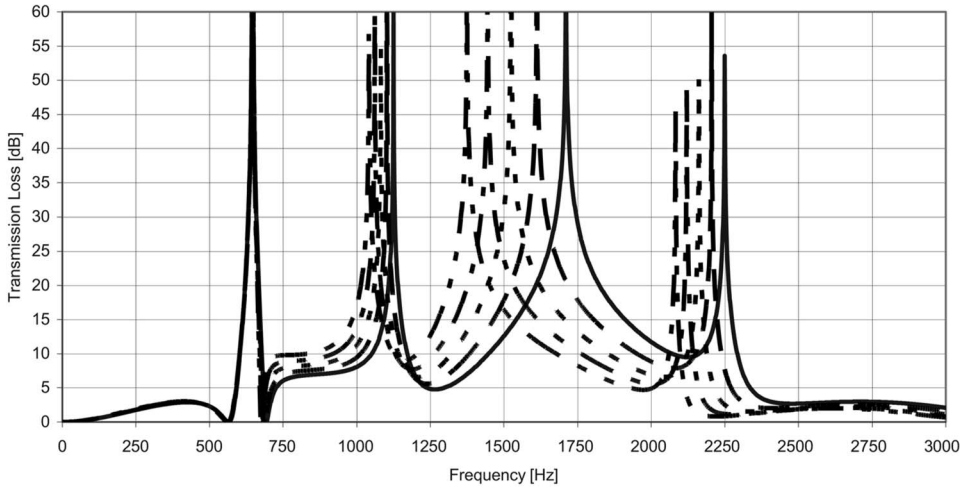


*Fig. 15—TL of the system consisting of a side branch duct and two Helmholtz resonators connected to the main duct. $h_{md}=36$ mm, $h_{hq}=36$ mm, $l_d=100$ mm, $h_{n1,n2}=12$ mm, $h_{hr1,hr2}=36$ mm, $l_{n1,n2}=15$ mm, $l_{hr1,hr2}=45$ mm. — $l_{hq}=198$ mm, — — $l_{hq}=204$ mm, – – – $l_{hq}=210$ mm, — – — $l_{hq}=216$ mm, — – – — $l_{hq}=222$ mm.*

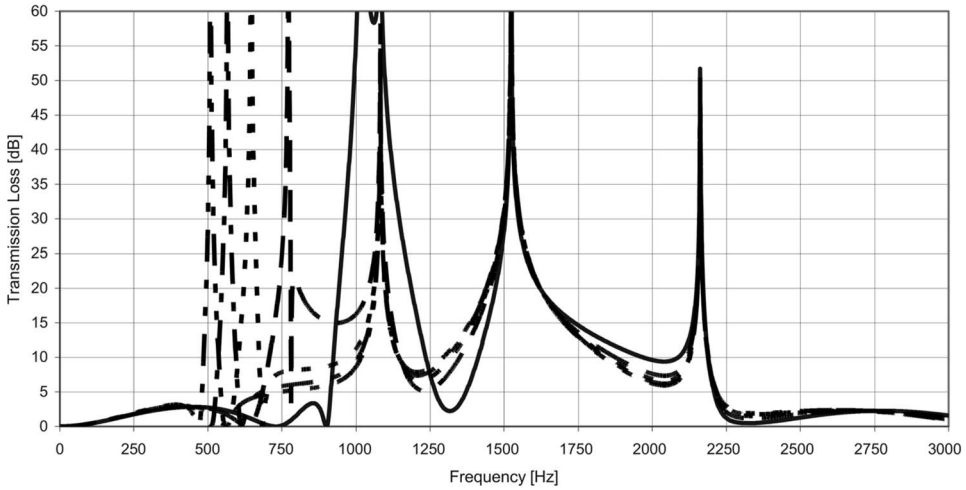


*Fig. 16—TL of the system consisting of a side branch duct modified with an expansion chamber and two Helmholtz resonators connected to the main duct. $h_{md}=36$ mm, $h_{hq}=36$ mm, $l_d=100$ mm, $h_{n1,n2}=12$ mm, $h_{hr1,hr2}=36$ mm, $l_{hr1,hr2}=45$ mm, $l_{hq}=200$ mm. — $l_{n1,n2}=5$ mm, — — $l_{n1,n2}=10$ mm, – – – $l_{n1,n2}=15$ mm, — – — $l_{n1,n2}=20$ mm, — – – — $l_{n1,n2}=25$ mm.*

=35 mm, $l_{hr1,hr2}$=40 mm, $l_{hr1,hr2}$=45 mm, $l_{hr1,hr2}$ =50 mm and $l_{hr1,hr2}$=55 mm. In these cases, the dimensions that are held constant are $h_{md}$=36 mm, $h_{hq}$ =36 mm, $l_d$=100 mm, $l_{hq}$=200 mm, $h_{n1,n2}$=12 mm and $l_{n1,n2}$=15 mm. Meaningful changes in the frequencies and TL levels are not observed in the figure, especially for those frequencies higher than 1000 Hz. The main effects of the length of the Helmholtz resonators are especially pronounced in the first TL peak. Comparison of our results shows that the longer the length, the lower the frequency of the first TL peak. This figure shows that the first TL peak essentially results from the resonators. From Eqn. (59), the resonance frequencies appear between 790 Hz for $l_{hr}$=35 mm and 620 Hz for $l_{hr}$=55 mm; the first TL peak is affected mainly by the length of the Helmholtz resonators. There are no significant changes in the frequency bandwidth of the first TL peak.

A similar analysis can be carried out using the results depicted in Fig. 18 for the geometries $h_{n1,n2}$ =6 mm, $h_{n1,n2}$=12 mm, $h_{n1,n2}$=18 mm, $h_{n1,n2}$=27 mm and $h_{n1,n2}$=36 mm. In these cases, the dimensions that are held constant are $h_{md}$=36 mm, $h_{hq}$=36 mm, $l_d$ =100 mm, $l_{hq}$=200 mm, $l_{n1,n2}$=15 mm, $h_{hr1,hr2}$ =36 mm and $l_{hr1,hr2}$=45 mm. Figure 18 shows the effect of diameters of the necks on the acoustic attenuation performance of the system. Increasing the neck diameter

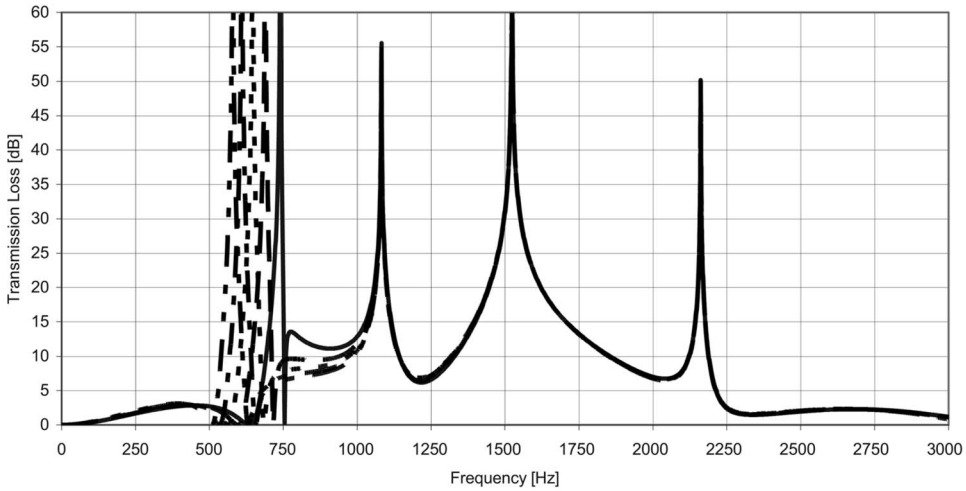


*Fig. 17—TL of the system consisting of a side branch duct modified with an expansion chamber and two Helmholtz resonators connected to the main duct. $h_{md}=36$ mm, $h_{hq}=36$ mm, $l_d=100$ mm, $l_{hq}=200$ mm, $h_{n1,n2}=12$ mm, $l_{n1,n2}=15$ mm. — $l_{hr1,hr2}=35$ mm, — — $l_{hr1,hr2}=40$ mm, – – – $l_{hr1,hr2}=45$ mm, — – — $l_{hr1,hr2}=50$ mm, — – – — $l_{hr1,hr2}=55$ mm.*

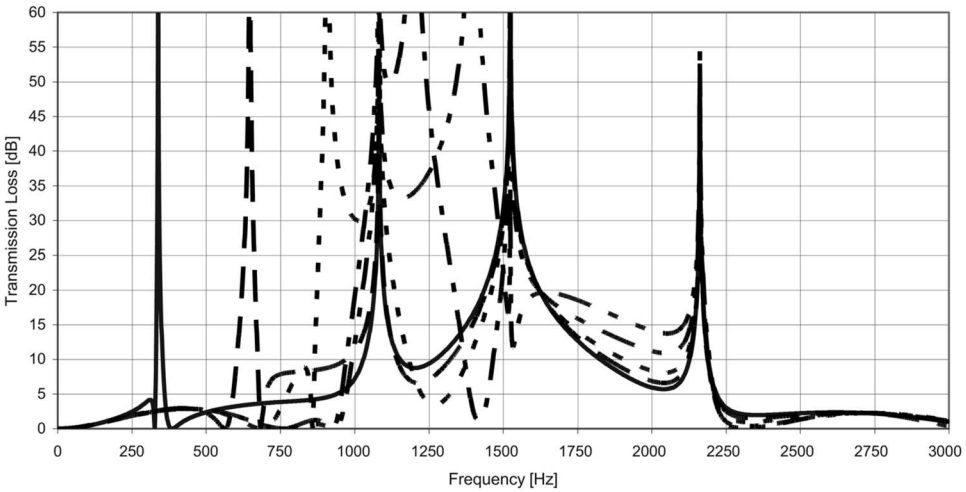


*Fig. 18—TL of the system consisting of a side branch duct modified with an expansion chamber and two Helmholtz resonators connected to the main duct. $h_{md}$=36 mm, $h_{hq}$=36 mm, $l_d$=100 mm, $l_{hq}$=200 mm, $l_{n1,n2}$=15 mm, $h_{hr1,hr2}$=36 mm, $l_{hr1,hr2}$=45 mm. — $h_{n1,n2}$=6 mm, — — $h_{n1,n2}$=12 mm, – – – $h_{n1,n2}$=18 mm, — – — $h_{n1,n2}$=27 mm, — – – — $h_{n1,n2}$=36 mm.*

shifts the first TL peak upwards and expands the frequency bandwidth. In the middle frequency range, the TL behavior of the system with extended necks is better than in the case of the directly connected resonators, except for certain narrow frequency bands associated with resonant peaks. From Eqn. (59), the resonance frequencies change between 340 Hz for $h_n$=6 mm and 2100 Hz for $h_n$=36 mm, and the first TL peak is affected mainly by the diameter of the neck.

In the next case, we investigate the diameters of the side branch duct and two Helmholtz resonators, as shown Fig. 19, for geometries $h_{hq,hr1,hr2}$=12 mm, $h_{hq,hr1,hr2}$=18 mm, $h_{hq,hr1,hr2}$=24 mm, $h_{hq,hr1,hr2}$=30 mm and $h_{hq,hr1,hr2}$=36 mm. In these cases, the dimensions that are held constant are $h_{md}$=36 mm, $l_d$=100 mm, $l_{hq}$=200 mm, $l_{n1,n2}$=15 mm, $l_{hr1,hr2}$=45 mm and $h_{n1,n2}$=12 mm. In each case, the diameters of both the resonators and the side branch duct are identical. The main effects of the size of the diameters are especially pronounced in the first TL peak. Comparison of the results shows that increasing the diameter shifts the first TL peak downwards and decreases the frequency bandwidth, whereas at the middle frequencies, the collapse of the TL behavior of the system associated with the size of diameters is evident, especially for the frequencies in between 1000 Hz and 1500 Hz. In addition, there

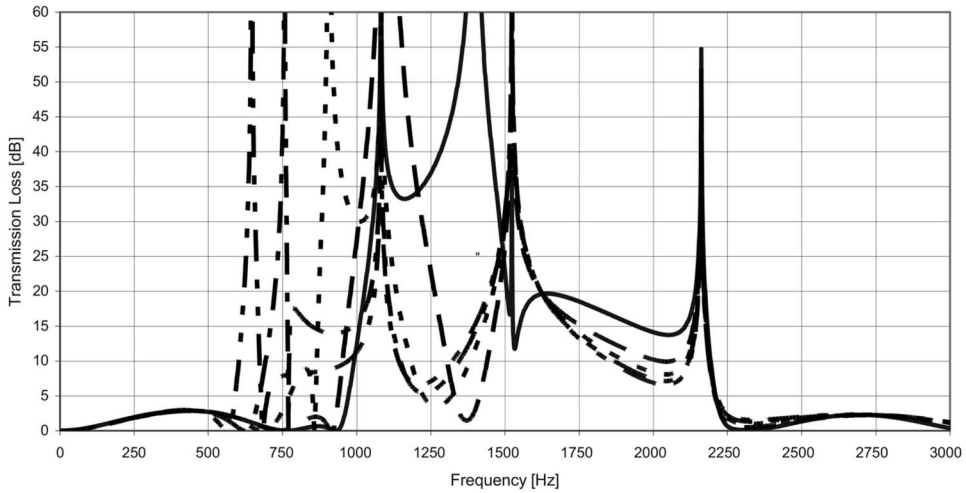


*Fig. 19—TL of the system consisting of a side branch duct modified with an expansion chamber and two Helmholtz resonators connected to the main duct. $h_{md}$=36 mm, $l_d$=100 mm, $l_{hq}$=200 mm, $l_{n1,n2}$=15 mm, $l_{hr1,hr2}$=45 mm, $h_{n1,n2}$=12 mm. — $h_{hq,hr1,hr2}$=12 mm, — — $h_{hq,hr1,hr2}$=18 mm, – – – $h_{hq,hr1,hr2}$=24 mm, — – — $h_{hq,hr1,hr2}$=30 mm, — – – — $h_{hq,hr1,hr2}$=36 mm.*

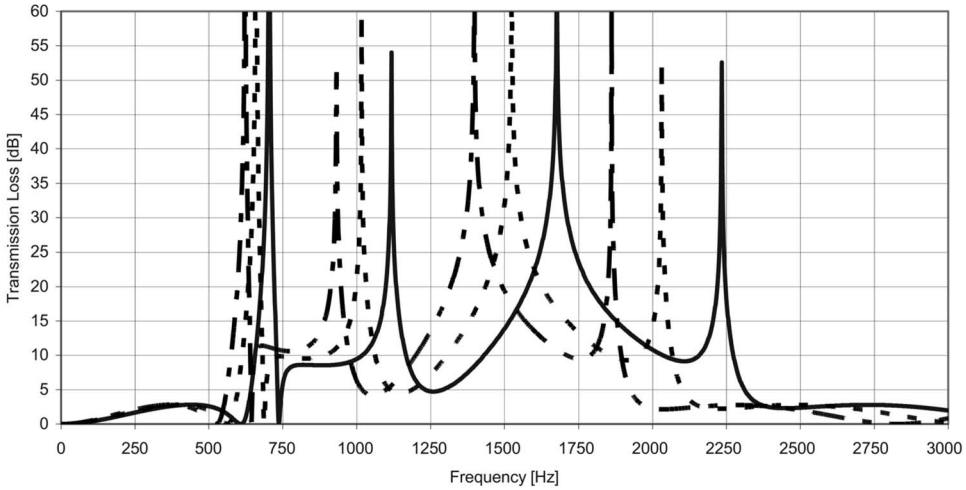


*Fig. 20—TL of the system consisting of a side branch duct modified with an expansion chamber and two Helmholtz resonators connected to the main duct. $h_{md}=36$ mm, $h_{hq}=36$ mm, $h_{n1,n2}=12$ mm, $h_{hr1,hr2}=36$ mm, $l_{hr1,hr2}=45$ mm, $l_{hq}=200$ mm, $l_{n1,n2}=15$ mm. — $l_d=100$ mm, – – – $l_d=110$ mm, — – — $l_d=120$ mm.*

is no meaningful change in the TL levels, especially for the frequencies higher than 2250 Hz. The initial resonance calculations from Eqn. (59) show that the resonance frequencies are intermediate, 2100 Hz for $h_{hr}=12$ mm and 690 Hz for $h_{hr}=36$ mm, and the first TL peak is affected mainly by the diameter of the neck. The frequency bandwidth of the first TL peak narrows while the resonance frequencies decrease.

Finally, the influence of the distance between the junction points is examined in Fig. 20 for geometries $l_d=100$ mm, $l_d=110$ mm and $l_d=120$ mm. In these cases, the dimensions that are held constant are $h_{md}=36$ mm, $h_{hq}=36$ mm, $h_{n1,n2}=12$ mm, $h_{hr1,hr2}=36$ mm, $l_{hr1,hr2}=45$ mm, $l_{hq}=200$ mm and $l_{n1,n2}=15$ mm. For the case in Fig. 20, the calculations show that the resonance frequencies are 690 Hz from Eqn. (59), 1130 Hz, 1700 Hz and 2250 Hz from Eqns. (56) and (57) for $l_d=100$ mm, 690 Hz from Eqn. (59), 1100 Hz, 1550 Hz and 1890 Hz from Eqns. (55)–(57) for $l_d=110$ mm and finally, 690 Hz from Eqn. (59), 1050 Hz, 1410 Hz and 2100 Hz from Eqns. (55)–(57) for $l_d=120$ mm. The results are consistent. Figure 20 shows that the change in the distance between the junction points does not affect the character of the TL curves, whereas the TL peaks shift downwards together with the increase in the distance, particularly at higher frequencies. There is no significant change in the TL levels and bandwidths.

In general, our results show that increasing the duct diameters leads to more extensive attenuation patterns. We generally found good agreement between the transfer matrix method and the finite element method results. As expected, some divergences were identified in regions near the cut-off frequency of the system.

In terms of applications, the solid models that we explored using the finite element method exhibit more detailed geometries and accurate dimensions than the models that we used with the transfer matrix method. Therefore, in some cases the deviations of the TL peaks seemed to result from the slight differences between the assumed dimensions and geometries. We conclude that the junction point is not a point in the solid models.

It is possible to use the transfer matrix method to predict the acoustic behavior of systems in the relatively low frequency range with geometries that are not too complex, at least in cases where the effects of higher order modes can be neglected.

## 4 CONCLUSIONS

We wished to construct an engineering design tool for the quick but moderately accurate determination of the TL of a system with two resonators connected to the main duct and the side branch duct modified with an expansion chamber. We derived an analytical model that uses the transfer matrix method for plane wave conditions and with no mean flow.

We apply our method to multiple different configurations, and we compare our numerical predictions with the results obtained using finite element methods. We discuss the limitations of our plane wave approach. In general, we find that the analytical and numerical results are in good agreement.

Numerical applications show that the 1D analytical approach yields satisfactorily accurate approximations in the 0–3000 Hz frequency range. Our results indicate that it is possible to manufacture a broadband muffler by using reactive type acoustic attenuation devices such as quarter wave resonators, Helmholtz resonators and side brunch ducts designed to certain optimal dimensions.

We note that the effect of extending the duct diameters is to widen the frequency bands of attenuation. Thus, we conclude that the method presented in this paper may be useful in examining the acoustical behavior of these structures in broadband noise control applications.

## 5 REFERENCES


1. N. S. Dickey and A. Selamet, "Helmholtz resonators: one-dimensional limit for small cavity length-to-diameter ratios", *J. Sound Vib.*, **195**, 512–517, (1996).
2. A. Selamet, P. M. Radavich, N. S. Dickey and J. M. Novak, "Circular concentric Helmholtz resonator", *J. Acoust. Soc. Am.*, **101**, 41–51, (1997).
3. A. Selamet and Z. L. Ji, "Circular asymmetric Helmholtz resonators", *J. Acoust. Soc. Am.*, **107**, 2360–2369, (2000).
4. A. Selamet and I. Lee, "Helmholtz resonator with extended neck", *J. Acoust. Soc. Am.*, **107**, 1975–1985, (2003).
5. C. B. Birdsong and C. J. Radcliffe, "A smart Helmholtz resonator", *ASME Forum on Active Noise Control, IMECE*, Dallas, (1997).
6. A. Selamet, P. M. Radavich and N. S. Dickey, "Multi-dimensional effects on silencer performance", *Noise Control Eng. J.*, **94**, 261–266, (1994).
7. A. Selamet and P. M. Radavich, "Effect of expansion chamber on the resonance frequency of side branches and Herschel-Quincke tubes", *ASME NCA* 22, 127–132, (1996).
8. A. Selamet and V. Easwaran, "Modified Herschel-Quincke tube: attenuation and resonance for n-duct configurations", *J. Acoust. Soc. Am.*, **102**, 164–169, (1997).
9. C. R. Fuller and D. A. Bies, "The effects of flow on the performance of a reactive acoustic attenuator", *J. Sound Vib.*, **62**, 73–92, (1979).
10. A. J. Torregrosa, A. Broatch and R. Payri, "A study of the influence of mean flow on the acoustic performance of Herschel-Quincke tubes", *J. Acoust. Soc. Am.*, **107**, 1874–1879, (2000).
11. Z. Zhichi, L. Song, T. Rui, G. Rui, D. Genhua and L. Peizi, "Application of Quincke tubes to flow ducts as a sound attenuation device", *Noise Control Eng. J.*, **46**, 245–255, (1998).
12. L. A. Brady, R. A. Burdisso and J. P. Smith, "Investigation of the Herschel-Quincke concept for the suppression of higher-order modes in a duct", *InterNoise99*, (1999).
13. R. F. Hallez, J. P. Smith and R. A. Burdisso, "Control of higher-order modes in ducts using arrays of Herschel-Quincke waveguides", *ASME Control of Vibration and Noise*, 1–8, (2000).
14. R. D. Stunk, "Silencer for hydraulic piston pump pressure pulsations", *Intern. Off-Highway and Powerplant Congress and Exposition, SAE Technical Paper Series 911759*, (1991).
15. C. C. Chen and M. C. Hastings, "Half-wavelength tuning cables for passive noise control in automotive power steering systems", *Active Control of Vibration and Noise, ASME DE-75*, 355–361, (1994).
16. S. N. Y. Gerges et al., "Muffler Modeling by Transfer Matrix Method and Experimental Verification", *J. of the Brazilian Society of Mechanical Science & Engineering*, **27**, 132–140, (2005).
17. E. P. Trochon, "A new type of silencers for turbocharger noise control", *SAE Technical Paper Series 01-1436*, (2001).
18. A. J. Graefenstein and W. Wenzel, "Herschel-Quincke Spiral: A new interference silencer", *SAE Technical Paper Series 01-1722*, (2003).
19. A. Selamet, N. S. Dickey and J. M. Novak, "The Herschel-Quincke tube: A theoretical, computational and experimental investigation", *J. Acoust. Soc. Am.*, **96**(5), 3177–3185, (1994).
20. M. Karlsson, R. Glav and M. Åbom, "The Herschel-Quincke tube: The attenuation conditions and their sensitivity to mean flow", *J. Acoust. Soc. Am.*, **124**(2), 723–732, (2008).
21. J. M. Desantes, A. J. Torregrosa, H. Climent and D. Moya, "Acoustic performance of a Herschel-Quincke tube modified with an interconnecting pipe", *J. Sound Vib.*, **284**, 283–298, (2005).
22. M. L. Munjal, *Acoustics of Ducts and Mufflers*, Wiley-Interscience, New York, (1987).